Journal of Sound and Vibration (2000) **231**(5), 1243–1256
doi:10.1006/jsvi.1999.2739, available online at http://www.idealibrary.com on IDEAL®

SOUND RADIATED FROM A CYLINDRICAL DUCT WITH KELLER'S GEOMETRICAL THEORY

S. T. HOCTER

Department of Mathematics, University of Keele, Keele, ST5 5BG, England

(*Received* 30 *June* 1999, *and in final form* 30 *September* 1999)

An exact solution to the problem of radiation from a cylindrical duct has been available using the Wiener–Hopf technique for many years, and a number of approximate methods can also be considered. When parameter spaces involving high frequency are required, it is possible to use ray-theory-based techniques to solve the problem. Keller proposed such a method, introducing a geometrical theory of diffraction (GTD) which extended the concept of geometrical optics to account for diffracted rays. When a ray propagates inside the duct, it will reflect off the duct rim creating a Keller cone of singly diffracted rays, allowing formulae to be obtained for the singly diffracted field using Keller's GTD. Expressions for the singly diffracted field are presented, and then compared with the exact solution for a range of parameters. The choice of parameters is governed by a set of mode angles which are used in describing geometrically how a ray propagates through the duct and out into free space.

© 2000 Academic Press

1. INTRODUCTION

An exact solution to the problem of sound radiation from a cylindrical duct has been available for many years. It has been derived using the Wiener–Hopf technique, firstly by Levine and Schwinger [1], who concentrated on the case of non-spinning modes. Weinstein [2] derived formulae for non-spinning modes at a similar time, but also presented some results for spinning modes. Later, workers to have used this technique include Lansing [3] and Homicz and Lordi [4]. Homicz and Lordi gave some examples of directivity patterns for a choice of modes relevant to the consideration of turbofans.

A number of approximate techniques exist which can be used to solve this problem. These range from the more complicated methods that require some knowledge of the exact solution, such as Weinstein's U function, to methods which take a more simplistic view of the problem. The best known of these is the Kirchhoff approximation, first identified by Tyler and Sofrin [5]. Instead of a semi-infinite cylindrical duct, a circular aperture in a plane screen is used and the radiated field is determined by a radiation integral evaluated over the aperture. The main disadvantage of this method is that it is not possible to determine the radiated field behind the duct rim. Weinstein's U function is derived by simplifying the kernel

0022-460X/00/151243 + 14 $35.00/0 © 2000 Academic Press

factors that occur when using the Wiener–Hopf technique by using the method of steepest descent. This results in an integral that can be expressed in terms of Weinstein's canonical U function whose parameters are dependent upon the particular kernel under consideration. When determining the accuracy of the approximations, the most common approach has been to determine the behaviour of the formula as $k_0 a$ is altered, since all these methods are high-frequency approximations. In following this approach, no consideration is made as to how an increase in frequency, while other parameters are fixed, will affect the ray structure of the propagating mode.

Using the modal angles described by Chapman [6], it is possible to express the propagating mode in terms of its geometrical progression along the duct. Some aspects of the ray structure have been derived by previous authors; in particular the mode ray angle, denoted here by θ_{ms}, has been shown to be particularly relevant [2, 7–9]. This angle is the polar mode angle of the propagating ray, and gives an approximate location for the main beam in the far field. To describe a ray in three dimensions, it is necessary to consider more than one angle. A ray propagating within the duct will form a piecewise linear helix within an outer annulus determined by the duct and an inner caustic cylinder. An azimuthal mode angle denoted by ϕ_{ms} is defined, where each segment of the helix is situated on planes tangent to the inner caustic at ϕ_{ms} to the meridional plane. When the ray strikes the rim of the duct, it will create a Keller cone of diffracted rays with a half-angle of $\pi/2 - \theta_m$, giving rise to the term "quiet-zone angle" to describe θ_m. The relevance of the mode ray angle, θ_{ms}, and the quiet zone angle, θ_m, can clearly be seen in the directivity plots obtained by Homicz and Lordi [4]. In an earlier paper [10], the author presented formulae for the radiated power per unit solid angle for approximate solutions obtained using Weinstein's U function and the Kirchhoff approximation. The accuracy of these formulae were then compared with the Wiener–Hopf solution in parameter spaces dependent upon the angles θ_{ms} and ϕ_{ms}.

When considering parameter spaces involving high frequency, it is possible to consider a ray-theory-based approach to the problem. An extension to geometrical optics was derived by Keller [11, 12] 40 years ago, and is known as Keller's geometrical theory of diffraction (GTD). In his classical papers, the problem of diffraction by a circular aperture in a plane screen with a normally incident plane wave was addressed. Keller hypothesized that when a plane wave strikes an edge at an oblique angle, a cone of diffracted rays results which is obtained by rotating the continuation of the incident ray about the tangent to the edge. A ray on this cone will strike the edge again leading to the creation of a cone of doubly diffracted rays. Thus, Keller also derived formulae for doubly and multiply diffracted rays. It is well known that GTD has limitations since this simple technique produces results that are not valid at shadow boundaries or caustics. Although not considered in this paper, there are a number of techniques which can be used to modify the GTD solution in these regions, though these add significant complexity to the formula. Kouyoumjian and Pathak [13] have determined a method which introduces a multiplicative factor to the diffraction coefficient that is zero at shadow boundaries, thereby cancelling out the singularity in the GTD method at that

region. An alternative approach involves the use of the ansatz of Ahluwalia *et al.* [14] which is a correction to the total field giving a different result in the region near a shadow boundary than that obtained by the Kouyoumjian and Pathak method. To deal with the breakdown of the formulae near caustics, Keller presented a formula valid for axial caustics, and this was extended to off-axial caustics by Albertsen *et al.* [15].

Since a propagating mode lies on a Keller cone after being diffracted by the rim of the duct, it is natural to introduce a co-ordinate system based on the Keller cones, which is derived in section 2. Expressions for the singly diffracted field can then be obtained using Keller's GTD. The accuracy of this solution can then be compared with the exact solution for the same parameters used in Reference [10].

2. CONAL CO-ORDINATES AND GEOMETRY

2.1. NOTATION

Consider an acoustic mode propagating in a semi-infinite cylindrical duct of radius a, denoted by A_{ms}, such that

$$p = p_0 \mathrm{e}^{-\mathrm{i}\omega t + \mathrm{i}m\phi_r + \mathrm{i}k_x x_0} \mathrm{J}_m(k_r r). \tag{1}$$

Here p_0 is proportional to the pressure amplitude, k_x is the axial wavenumber and k_r is the radial wavenumber. The incident mode must be a solution of the wave equation, which gives the relationship $k_x = \sqrt{k_0^2 - k_r^2}$. This is an important expression that is used to determine whether a mode is cut-on (or propagating), when k_x is real, or if a mode is cut-off. The boundary condition $\partial p/\partial r = 0$ on $r = a$ is used to show that $j'_{ms} = k_r a$, where $\mathrm{J}'_m(j'_{ms}) = 0$. This introduces the radial order, s, of the propagating mode and one should note that $k_x \equiv k_x^{ms}$. The notation A_{ms} is used to determine the azimuthal and radial order defining a particular incident mode, illustrated for the selection of radiated field directivity patterns presented later. The Bessel identity $\mathrm{J}_m(z) = \frac{1}{2}(\mathrm{H}_m^{(1)}(z) + \mathrm{H}_m^{(2)}(z))$ is used to re-write the incident mode so that it now only contains the portion propagating outwardly in a radial direction (the first term in the parentheses here). Hence, omitting the superscript (1) from $\mathrm{H}_m^{(1)}$ hereafter, and with $\phi'_r = \phi_r - \phi$ one may write

$$p = \frac{p_0}{2} \mathrm{e}^{-\mathrm{i}\omega t + \mathrm{i}m\phi + \mathrm{i}m\phi'_r + \mathrm{i}k_x x_0} \mathrm{H}_m\left(\frac{j'_{ms}}{a} r\right). \tag{2}$$

A modal ray structure is used to describe the propagation of the ray along the duct, and the angles θ_m, θ_{ms} and ϕ_{ms} are introduced, as defined by Chapman [6], where

$$\sin\theta_m = \frac{m}{k_0 a}, \qquad \sin\theta_{ms} = \frac{j'_{ms}}{k_0 a}, \qquad \sin\phi_{ms} = \frac{m}{j'_{ms}}. \tag{3}$$

These angles are illustrated in Figure 1, whilst a comprehensive description of their relationship to the propagating mode is given in reference [10].

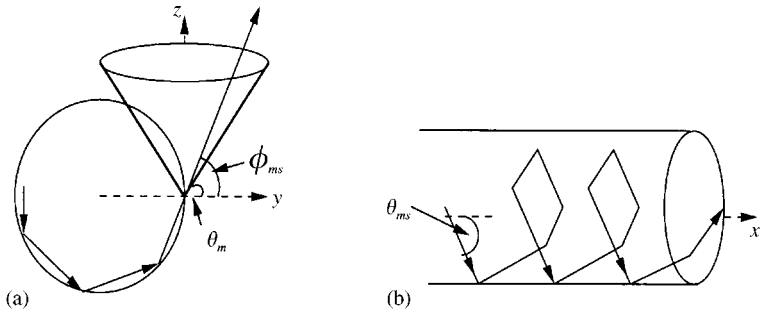

Figure 1. Ray geometry: (a) End view of duct showing Keller cone at angle θ_m to the y-axis and portion of propagating ray at angle ϕ_{ms} to the y-axis, (b) Side view of duct showing ray to be a piecewise linear helix with each segment at angle θ_{ms} to duct axis.

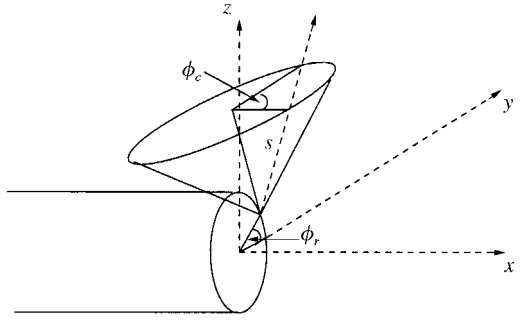

Figure 2. 3-D conal co-ordinates (s, ϕ_r, ϕ_c) with Cartesian co-ordinates (x, y, z).

2.2. CO-ORDINATE SYSTEM

When the ray strikes the rim of the duct, it creates a Keller cone of diffracted rays which is obtained by extending the incident ray and rotating it about the tangent to the rim at the point of diffraction. It is therefore natural to define a co-ordinate system based upon the Keller cone. To describe a position in space, we use the co-ordinates (s, ϕ_r, ϕ_c) where s represents the length along the cone from its vertex, ϕ_r gives the location of the vertex of the cone on the duct rim and ϕ_c measures the angle around the cone, as illustrated in Figure 2. A point on the cone described using conal co-ordinates can be related to Cartesian co-ordinates by

$$x = s\cos\theta_m\cos\phi_c,$$

$$y = s(\cos\theta_m\sin\phi_c\cos\phi_r - \sin\theta_m\sin\phi_r) + a\cos\phi_r,$$

$$z = s(\cos\theta_m\sin\phi_c\sin\phi_r + \sin\theta_m\cos\phi_r) + a\sin\phi_r. \qquad (4)$$

If we consider a ray originating at a point on the rim given by $x_0 = 0$, $y_0 = a\cos\phi_r$, $z_0 = a\sin\phi_r$, the distance from the rim to a point in space can be found using

$s^2 = (x - x_0)^2 + (y - y_0)^2 + (z - z_0)^2$. Noting that $s \gg a$, an expression for s in the far field expressed in spherical co-ordinates, (R, θ, ϕ), can be obtained using the binomial theorem such that

$$s \approx R - a \sin\theta \cos\phi_r'. \tag{5}$$

Here s is the distance to a point P measured from the duct rim, whereas R is measured from the centre of the duct rim. For large R, one can clearly see that $s \approx R$, as expected. Comparing this with the conal co-ordinate system introduced above, and recalling that $x = R\cos\theta$, it can be noted that $\cos\theta \approx \cos\theta_m \cos\phi_c$ in the far field. Hence

$$\cos\theta_m \sin\phi_c \approx \pm\sqrt{\cos^2\theta_m - \cos^2\theta}. \tag{6}$$

Substituting the expressions for the conal co-ordinates given in equation (4) into $R^2 = x^2 + y^2 + z^2$ gives $R^2 = s^2 + 2sa\cos\theta_m \sin\phi_c + a^2$. Expanding this equation using the binomial theorem leads to

$$R \approx s + a\cos\theta_m \sin\phi_c. \tag{7}$$

To $O(1)$, equations (5) and (7) agree provided

$$\cos\phi_r' = \frac{1}{\sin\theta}\cos\theta_m \sin\phi_c \approx \pm\frac{1}{\sin\theta}\sqrt{\cos^2\theta_m - \cos^2\theta} \tag{8}$$

using equation (6) to simplify ϕ_r' in the far field. This relationship can also be derived by expanding the $O(1)$ term in equation (5) and substituting the terms in ϕ with expressions obtained from the y and z terms of the conal co-ordinates when $s \approx R$.

2.3. EXACT SOLUTION

The exact solution used to determine the accuracy of the Keller formula is obtained using the Wiener–Hopf technique, and expressed as a radiated power per unit solid angle such that

$$\mathscr{P}_{wh}(\theta) = \frac{P_i^{wh} k_0 k_x^s}{\pi^2 (k_0\cos\theta - k_x^s)^2} \frac{\mathrm{J}_m'(k_0 a \sin\theta)}{|\mathrm{H}_m'(k_0 a \sin\theta|} \prod_{\substack{n=1 \\ \neq s}}^{N} \frac{k_x^n + k_x^s}{k_x^n - k_x^s}$$

$$\times \prod_{n=1}^{N} \frac{k_x^n - k_0\cos\theta}{k_x^n + k_0\cos\theta} \, \mathrm{e}^{\Re[S(k_x^s a) - S(k_0 a\cos\theta)]}, \tag{9}$$

where N denotes the radial order of the highest propagating mode and P_i^{wh} is the power of the incident mode, of the form stated in equation (1). The function $\Re[S]$ is

given by

$$\Re[S(\zeta)] = \frac{1}{\pi} P \int_{-k_0 a}^{k_0 a} \frac{\Omega(\kappa a)}{k' - \zeta} \, \mathrm{d}k', \qquad k' = ka, \tag{10}$$

where numerical integration is performed using NAG libraries, and the integral is taken in its Cauchy principal value sense. The Ω function is defined by

$$\Omega(k) = \tan^{-1} \frac{\mathrm{Y}'_m(k)}{\mathrm{J}'_m(k)} \pm \frac{\pi}{2}, \qquad \begin{cases} (+), & m = 0, \\ (-), & m \neq 0. \end{cases} \tag{11}$$

When calculating the Ω function it is necessary to include its phase, which is given by $\Omega(0) = 0$, $\Omega(j'_{ms}) = (s-1)\pi$ when $m \neq 0$. However, for $m = 0$, one must use $\Omega(j'_{ms}) = s\pi$.

3. ANALYSIS OF PROBLEM

Keller's geometrical theory of diffraction gives a representation of the singly-diffracted field using a canonical diffraction coefficient determined from Sommerfeld's exact solution for diffraction of a plane scalar wave by a half-plane. Using equation (20) of reference [12] the singly diffracted field can be represented by

$$p_{e1} = D p_i [s(1 + \rho_1^{-1} s)]^{-1/2} \mathrm{e}^{\mathrm{i}k_0 s}. \tag{12}$$

The incident mode is evaluated at the point of diffraction, which at any position on the rim is given by $x_0 = 0$ and $r = a$, greatly simplifying that part of the expression. D is the canonical diffraction coefficient, given by

$$D = \frac{-\mathrm{e}^{\mathrm{i}\pi/4}}{2(2\pi k_0)^{1/2} \sin\beta} \left[\sec\frac{1}{2}(\theta_k - \alpha) + \sec\frac{1}{2}(\theta_k + \alpha) \right],$$

where β is the angle between the incident ray and the edge and θ_k is the angle between the rim and the projection of the diffracted ray in a plane normal to the edge at the point of diffraction, that is, the r–x plane. The angle α denotes the angle between the rim and the incident ray in a plane normal to the edge at the point of diffraction. The ray exits the duct at θ_{ms} to the duct axis, giving $\alpha = \theta_{ms}$. The definition of these angles gives a diffraction coefficient slightly different from that used by Keller [11, 12] where θ_K and α_K are measured from the normal to the edge. That is, $\theta_K = \theta_k + \pi/2$, with the subscript K referring to the definition of the angles used by Keller; the same substitution is used for α_K. At a point in space towards the

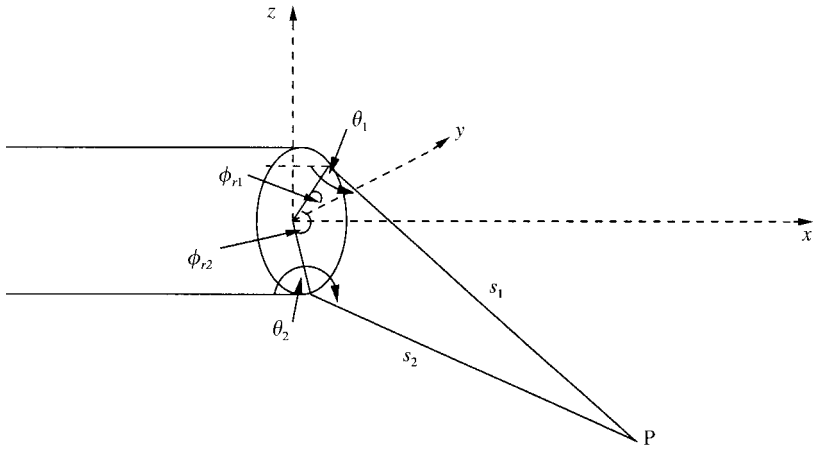

Figure 3. Definition of angles and distances used in diffraction method, where θ_1 and θ_2 are angles measured between the rim and the projection of the diffracted ray in the r–x plane.

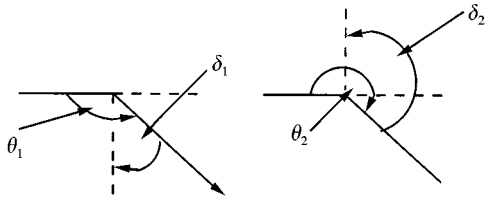

Figure 4. Definition of angle δ used in diffraction coefficient.

front of the duct rim, there will be contributions to the radiated field from two points on the rim using the geometry described in Figure 3. In equation (12), $-\rho_1$ is the distance from the point of diffraction to a caustic, and for the mode angles defined above it is given by

$$\rho_1^{-1} = -\frac{\cos\delta}{a\sin^2\beta}, \tag{13}$$

where δ is defined as the angle between the diffracted ray and the normal to the edge (pointing towards the centre of curvature). The definition of $\delta_{1,2}$ and its relationship to $\theta_{1,2}$ is illustrated in Figure 4. As before, this angle is measured from the projection of the diffracted ray in the r–x plane. Then, at a point in space, P, towards the front of the duct, the singly diffracted field can be written as

$$p_{e1,2}(P) = -\frac{p_0 e^{im\phi - i\omega t}}{4(2\pi k_0)^{1/2}} \frac{e^{im\phi'_{r1} + ik_0(x_0 + s_1) + i\pi/4}}{[s_1(\sin^2\beta + (s_1/a)\sin\theta_1)]^{1/2}} H_m(k_r r)$$

$$\times\left[\sec\frac{1}{2}(\theta_1 - \theta_{ms}) + \sec\frac{1}{2}(\theta_1 + \theta_{ms})\right]$$

$$-\frac{p_0 e^{im\phi - i\omega t}}{4(2\pi k_0)^{1/2}} \frac{e^{im\phi'_{r2} + ik_0(x_0 + s_2) + i\pi/4}}{[s_2(\sin^2\beta + (s_2/a)\sin\theta_2)]^{1/2}} H_m(k_r r)$$

$$\times\left[\sec\frac{1}{2}(\theta_2 - \theta_{ms}) + \sec\frac{1}{2}(\theta_2 + \theta_{ms})\right]. \tag{14}$$

To express the formula in the far field, let $s_1 \approx R + a\sqrt{\cos^2\theta_m - \cos^2\theta}$, $s_2 \approx R - a\sqrt{\cos^2\theta_m - \cos^2\theta}$, $\phi'_{r1} \approx \cos^{-1}(\sqrt{\cos^2\theta_m - \cos^2\theta}/\sin\theta)$ and $\phi'_{r2} \approx \pi - \cos^{-1}(\sqrt{\cos^2\theta_m - \cos^2\theta}/\sin\theta)$ using the far-field approximations to the conal co-ordinates described earlier. To ensure that the definition of θ agrees with that used in a previous paper [10], let $\theta_1 \approx \pi + \theta$, $\theta_2 \approx \pi - \theta$. Finally, since $s \approx R \gg a$, one may also write

$$\left[s_1\left(\sin^2\beta + \frac{s_1}{a}\sin\theta_1\right)\right]^{1/2} \approx i\left(\frac{R^2}{a}\sin\theta\right)^{1/2},$$

$$\left[s_2\left(\sin^2\beta + \frac{s_2}{a}\sin\theta_2\right)\right]^{1/2} \approx \left(\frac{R^2}{a}\sin\theta\right)^{1/2}. \tag{15}$$

Note that a factor $-i\pi/2$ occurs in the phase of a ray originating at the θ_1 position indicating that it has crossed the caustic at θ_m in reaching a point P below the axis in the loud zone. The location of the caustics and shadow boundaries in the far field is illustrated in Figure 5. Substituting the various far-field identities into equation (14) gives the singly diffracted field as

$$p_{e1,2}(P) = \frac{p_0 a^{1/2} H_m^{(1)}(j'_{ms})}{4(2\pi k_0 \sin\theta)^{1/2} R} \exp\left(im\phi - i\omega t + ik_0 R + \frac{im\pi}{2}\right)(e^{i\xi} - e^{-i\xi})$$

$$\times\left[\operatorname{cosec}\frac{1}{2}(\theta + \theta_{ms}) + \operatorname{cosec}\frac{1}{2}(\theta - \theta_{ms})\right],$$

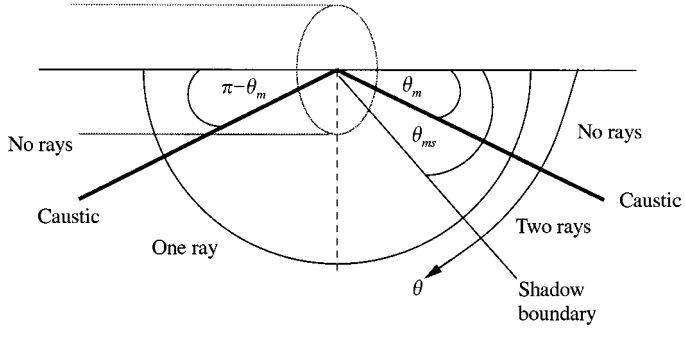

Figure 5. Location of caustics and shadow boundaries in the far field.

$$\xi = k_0 a\sqrt{\cos^2\theta_m - \cos^2\theta} + m\cos^{-1}\left(\frac{1}{\sin\theta}\sqrt{\cos^2\theta_m - \cos^2\theta}\right) - \frac{m\pi}{2} - \frac{\pi}{4}. \tag{16}$$

Directivity formulae are obtained by considering the radiated power per unit solid angle, where $\mathscr{P}_e(P) = (1/2\rho_0 c)|p_e|^2 R^2$, and then expressing this in terms of the power of the incident mode such that

$$\mathscr{P}_{e1,2}(P) = \frac{P_i}{2\pi^2 k_0 a \sin\theta\cos\theta_{ms}\cos^2\phi_{ms}}\left[\operatorname{cosec}\frac{1}{2}(\theta+\theta_{ms}) + \operatorname{cosec}\frac{1}{2}(\theta-\theta_{ms})\right]^2$$

$$\times\cos^2\left(k_0 a\sqrt{\cos^2\theta_m - \cos^2\theta} + m\cos^{-1}\left(\frac{1}{\sin\theta}\sqrt{\cos^2\theta_m - \cos^2\theta}\right) - \frac{m\pi}{2} + \frac{\pi}{4}\right)$$

$$\times[1 + 4/\pi^2 j'^2_{ms}\cos^2\phi_{ms}\mathrm{J}_m^2(j'_{ms})(\mathrm{J}_m^2(j'_{ms}) + \mathrm{Y}_m^2(j'_{ms}))]^{-1}, \tag{17}$$

where

$$P_i = \frac{\pi p_0^2 a^2}{8c\rho_0}\cos\theta_{ms}\cos^2\phi_{ms}(\mathrm{J}_m^2(j'_{ms}) + \mathrm{Y}_m^2(j'_{ms}))$$

$$\times[1 + 4/\pi^2 j'^2_{ms}\cos^2\phi_{ms}\mathrm{J}_m^2(j'_{ms})(\mathrm{J}_m^2(j'_{ms}) + \mathrm{Y}_m^2(j'_{ms}))]. \tag{18}$$

Note that P_i is different from the incident power used for the exact solution, and for numerical computation P_i can be expressed as a function of P_i^{wh}, with $P_i^{wh} = 1$ for the directivity plots included here.

To obtain an expression for the field behind the duct rim, note that there will be contributions to the radiated field from one of the terms in equation (16). Then, using the approach used above, the radiated powder per unit solid angle behind the duct is given by

$$\mathscr{P}_{e1,1}(P) = \frac{P_i[\operatorname{cosec}\frac{1}{2}(\theta+\theta_{ms}) + \operatorname{cosec}\frac{1}{2}(\theta-\theta_{ms})]^2}{8\pi^2 k_0 a\sin\theta\cos\theta_{ms}\cos^2\phi_{ms}}$$

$$\times[1 + 4/\pi^2 j'^2_{ms}\cos^2\phi_{ms}\mathrm{J}_m^2(j'_{ms})(\mathrm{J}_m^2(j'_{ms}) + \mathrm{Y}_m^2(j'_{ms}))]^{-1}. \tag{19}$$

The formulae obtained thus far are only valid in the loud zone; that is the region $\theta_m \leqslant \theta \leqslant \pi - \theta_m$. Outside this region equations (17) and (19) become complex. However, by noting that it is possible to write $\sqrt{\cos^2\theta_m - \cos^2\theta} = \mathrm{i}\sqrt{\cos^2\theta - \cos^2\theta_m}$, where the expression in the $\sqrt{}$ is positive in the quiet zone, equation (16) can be re-formulated in the quiet zone. A formula for the singly

diffracted field in the forward quiet zone is then obtained, such that

$$\mathscr{P}_{eq1,2}(P) = \frac{P_i}{4\pi^2 k_0 a \sin\theta}\left[\operatorname{cosec}\frac{1}{2}(\theta+\theta_{ms}) + \operatorname{cosec}\frac{1}{2}(\theta-\theta_{ms})\right]^2$$

$$\times \frac{\cosh(2m\ln(1/\sin\theta[\sqrt{\cos^2\theta-\cos^2\theta_m}+\sin\theta_m]) - 2k_0 a\sqrt{\cos^2\theta-\cos^2\theta_m})}{\cos\theta_{ms}\cos^2\phi_{ms}[1+4/\pi^2 j'^2_{ms}\cos^2\phi_{ms}\mathrm{J}^2_m(j'_{ms})(\mathrm{J}^2_m(j'_{ms})+\mathrm{Y}^2_m(j'_{ms}))]} \tag{20}$$

and the radiated power per unit solid angle in the rearward quiet zone is given by

$$\mathscr{P}_{eq1,1}(P) = \frac{P_i}{8\pi^2 k_0 a \sin\theta}\left[\operatorname{cosec}\frac{1}{2}(\theta+\theta_{ms}) + \operatorname{cosec}\frac{1}{2}(\theta-\theta_{ms})\right]^2$$

$$\times \frac{\exp[2k_0 a\sqrt{\cos^2\theta-\cos^2\theta_m} - 2m\ln(1/\sin\theta[\sqrt{\cos^2\theta-\cos^2\theta_m}+\sin\theta_m])]}{\cos\theta_{ms}\cos^2\phi_{ms}[1+4/\pi^2 j'^2_{ms}\cos^2\phi_{ms}\mathrm{J}^2_m(j'_{ms})(\mathrm{J}^2_m(j'_{ms})+\mathrm{Y}^2_m(j'_{ms}))]}. \tag{21}$$

For the formula in the rearward quiet zone, one takes a ray originating from the θ_2 position, since it can be seen from Figure 3 that to the rear of the duct, a ray from the θ_1 position will be "trapped" within the duct contributing towards the reflected field.

4. DISCUSSION OF RESULTS

The accuracy of the singly diffracted field, derived with the GTD method as presented above can be compared to the exact solution for any permissible combination of the mode angles θ_m, θ_{ms} and ϕ_{ms}. However, the choice of angles is limited by the relationship $m < j'_{ms} < k_0 a$ which is determined by properties of Bessel functions and the constraint upon propagating modes. Clearly, from a geometrical point of view, it would be expected that $\theta_{ms} > \theta_m$, which simply expresses that the principal lobe must be in the loud zone. The numerical results presented in Figure 6 show a comparison of the exact solution (solid line) and the GTD approximation (dashed line) for a number of values of θ_{ms} and ϕ_{ms}, with results included for $\phi_{ms} = 0^\circ$ to illustrate the case of non-spinning modes. The results are represented by radiated field directivity patterns showing radiated power per unit solid angle where $\theta = 90^\circ$ is perpendicular to the duct rim, and $\theta > 90^\circ$ represents the field behind the duct rim plane.

Throughout the directivity patterns, some common themes can be observed. As expected, the formulae are singular at θ_{ms}, which corresponds to the shadow boundary of geometrical optics. It was expected that there would be a broad region where the approximation degrades, but adding contributions from two rays that

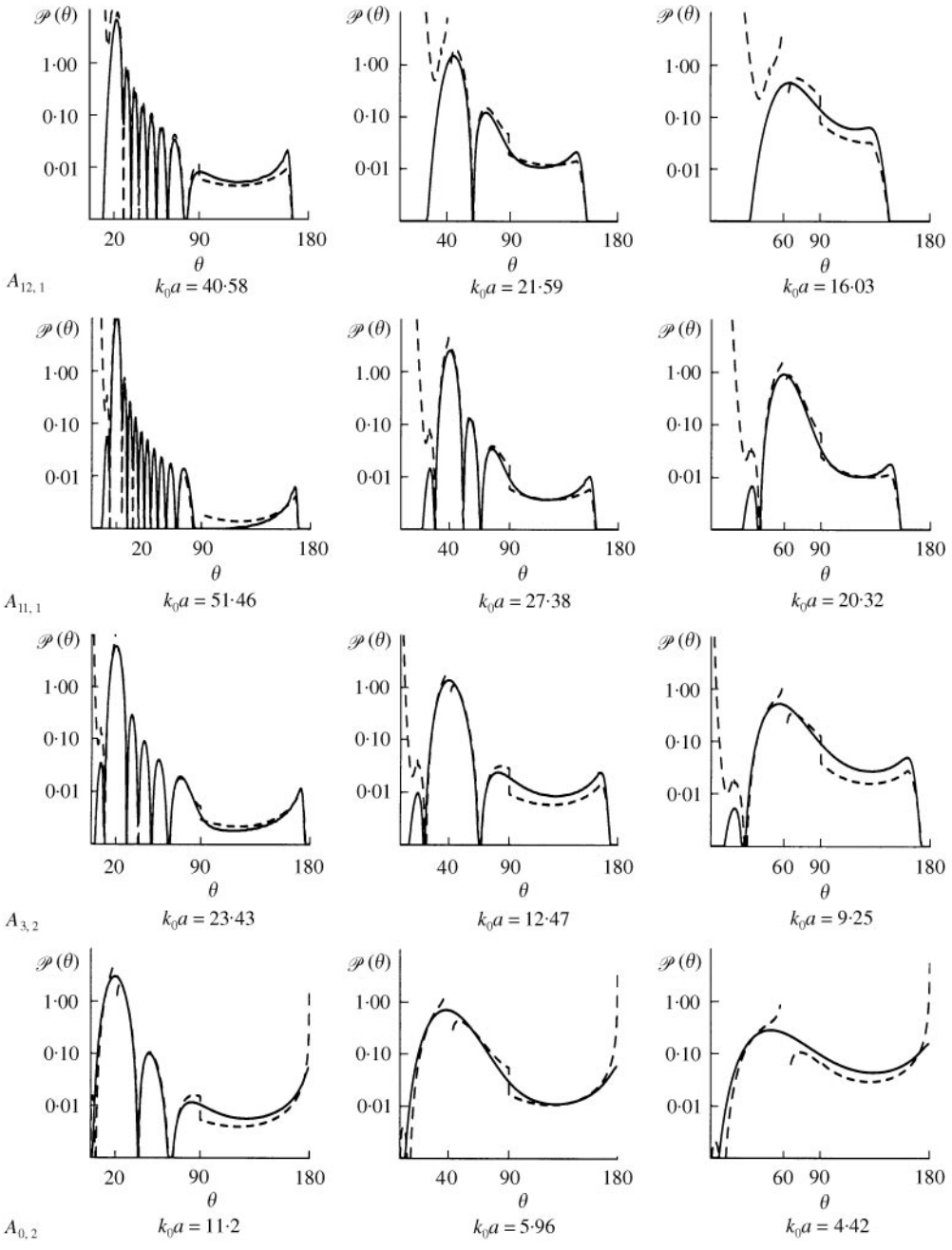

Figure 6. Directivity plots of radiated power per unit solid angle showing exact solution (solid line) and singly diffracted GTD solution (dashed line). The parameters used are $\theta_{ms} \approx 20^\circ$, 40°, 60° and $\phi_{ms} \approx 0^\circ$, 20°, 40° and 60°.

are singular at the mode ray angle limits the adverse effects of the singularity, except in a region very close to θ_{ms}. For the directivity patterns of the spinning modes, the GTD formulae are applicable to within a region of 1° either side of the shadow boundary. This region is slightly larger for the non-spinning modes, although still

not excessively so. Furthermore, at the transition between the loud and quiet zone, the presence of a caustic affects the accuracy of the results. The effect of the caustic at θ_m can also be seen for the $m = 0$ case where the GTD approximation fails near the forward axis, though this behaviour is not as severe as one increases $k_0 a$. The discontinuity at the sideline which results from switching between the two-ray and one-ray formula is also apparent. Fortunately, corresponding to the behaviour observed with the U approximation, [10], this discontinuity decreases as one increases $k_0 a$. The approach used in taking a complex ray in the rearward quiet zone has produced the exponential drop-off at $\pi - \theta_m$ as predicted by the exact solution. However, the behaviour has not been reproduced in the forward loud zone and further consideration of the problem in this region is required.

This ray-theory-based approach to the problem is particularly suitable for high-frequency approximations, as shown empirically by the lack of accuracy for small $k_0 a$ that diminishes as $k_0 a$ increases. This pattern is apparent for all choices of ϕ_{ms}. Moreover, this also corresponds to increasing θ_{ms}, which is equivalent to varying $k_0 a$ such that the frequency of the propagating mode approaches cut-off, i.e., $k_0 a \approx j'_{ms}$. In this case, the incident ray propagates almost perpendicularly to the duct axis, so that it diffracts from the rim of the duct at grazing incidence. It has also been noted by Yee and Felsen [16] that problems arise when using ray theory in situations with propagating rays striking an edge at grazing incidence. The directivity patterns illustrate that increasing ϕ_{ms} has no significant effects on the accuracy of the GTD approximation, an observation also noted for both the U approximation and the Kirchhoff approximation. However, for sufficiently high values of ϕ_{ms}, corresponding to the whispering gallery modes, we are unable to obtain numerical results for the exact solution to allow for comparison with the singly diffracted field.

In general, comparing these results with those obtained for other approximations [10], the singly diffracted field is a better approximation than the Kirchhoff method, although is not as accurate as the U approximation, provided we are far from cut-off. Expressions for the doubly and multiply diffracted field have also been obtained, and as expected, these do not contribute a significant amount to the total field. Since the incident ray lies in the duct rim plane, it is necessary to use the modified diffraction coefficient stated by Keller [12], and the shadow boundary for the multiply diffracted formula is now located at the sideline. Finally, behind the duct rim, assuming that there is a contribution from one ray for the radiated field does indeed give the board lobe expected, although for some parameters the singly diffracted field is separated from the exact solution. This phenomenon was also observed with the U approximation, although it should be borne in mind that these curves are plotted on logarithmic scales so that the loss in accuracy decreases as θ_{ms} decreases, corresponding to increase $k_0 a$.

5. CONCLUSIONS

This paper presents formulae that express the sound radiated from a semi-infinite cylindrical duct with Keller's geometrical theory of diffraction. The directivity patterns presented illustrate that the singly diffracted field is a good

approximation to the Wiener–Hopf solution in most regions in the far field, even though the technique is much simpler to derive and compute than the exact solution. A set of numerical results for fixed ϕ_{ms} and θ_{ms} are included, although any set of results can be determined using the expressions presented previously. In general, the singly diffracted field is a good approximation to the exact solution, provided that one notes that ray-theory-based methods are only suitable for high frequency approximations. Expressions for the doubly diffracted field can be easily obtained using the modified diffraction coefficients, where the incident field is obtained from the expressions for the singly diffracted field presented here. This method can then be repeated to determine the total multiply diffracted field. Although not shown, it can be observed that the contribution from the total multiply diffracted field is significantly less than the singly diffracted field. In fact, the doubly diffracted field alone is of $O((k_0 a)^{-4})$-factors of $(k_0 a^3)^{-1/2}$ from the incident field and ${k_0}^{-3/2}$ from the diffraction coefficient occur. These factors are then squared when the radiated power per unit solid angle is determined. Similarly, factors of $a^{1/2}$ from the spreading factor and a^2 from the incident power P_i contribute to the $1/(k_0 a)^4$ behaviour.

When using Keller's method, it must be born in mind that it does have well-known limitations; failing to predict the field correctly at shadow boundaries and caustics. Fortunately, a great deal of research exists to correct the discrepancies in these regions, as noted earlier. These do add some significant complication to the form of the results and a balance between the simple nature of the expressions derived here and the more complicated forms required in fairly small regions in the far field needs to be determined. Further investigation into the "blow-up" in the forward loud zone is also required since this region alone does not exhibit the expected behaviour. The effect of the geometry of the propagating mode is clearly shown here, with the approximation ceasing to be accurate for large θ_{ms}. In this case, that corresponds both to modes near cut-off, and to small $k_0 a$. Interestingly, no discernible pattern in the accuracy of the approximation can be observed for ray geometry approaching the creeping structure of whispering gallery modes. This could simply be a result of the choice of ϕ_{ms} being limited by the possible results obtained from the exact solution, though another reason could be that the failings of Keller's method are only specifically related to θ_m and θ_{ms}. Further results are presented by the author [17] including numerical results for various other parameter spaces and analytical formulae for the doubly and multiply diffracted field.

Now that the basic cylindrical duct problem has been addressed, it is possible to consider the addition of many of the extra complications to the problem that exist. For example, a geometrical solution could be considered that encompasses bell mouth ducts, duct liners, etc. It could be possible to consider the effects of mean flow using the Doppler factors presented by Chapman [7]. How the multiply diffracted field is related to the U approximation using the approach outlined by Bowman *et al.* [18, p. 46, 47] could also be considered. For the case of the plane parallel waveguide, they asymptotically expanded the U approximation for large $k_0 a$, showing that it gives an equivalent representation of the multiply diffracted field.

ACKNOWLEDGMENTS

The author would like to thank Dr C. J. Chapman for his advice throughout this work. This work was carried out while the author was in receipt of an EPSRC studentship, and was partially supported by an E. U. ERASMUS-SOCRATES grant. The author would also like to thank Dr Börje Nilsson of MASDA, Växjö University for his gracious hospitality.

REFERENCES

1. H. Levine and J. Schwinger 1943 *Physical Review* **73**, 383–406. Radiation of sound from a circular pipe.
2. L. A. Weinstein 1969 *The Theory of Diffraction and the Factorization Method* (*Generalized Wiener–Hopf Technique*). *Golem.*
3. D. L. Lansing 1970 *Analytical Methods in Aircraft Aerodynamics* NASA SP-228, 323–334. Exact solution for radiation of sound from a semi-infinite circular duct with application to fan and compressor noise.
4. G. F. Homicz and J. A. Lordi 1975 *Journal of Sound and Vibration* **41**, 283–290. A note on the radiative directivity patterns of duct acoustic modes.
5. J. M. Tyler and T. G. Sofrin 1962 *Society of Automotive Engineers Transactions* **70**, 309–332. Axial flow compressor noise studies.
6. C. J. Chapman 1994 *Journal of Fluid Mechanics* **281**, 293–311. Sound radiation from a cylindrical duct. Part 1. Ray structure of the duct modes and of the external field.
7. C. J. Chapman 1996 *Journal of Fluid Mechanics* **313**, 367–380. Sound radiation from a cylindrical duct. Part 2. Source modelling, nil-shielding directions, and the open-to-ducted transfer function.
8. E. J. Rice 1978 *AIAA Journal* **16**, 906–911. Multimodal far-field radiation pattern using mode cutoff ratio.
9. E. J. Rice, M. F. Heidmann and T. G. Sofrin 1979 *Paper no. AIAA*-79-0183, *Presented at the American Institute of Aeronautics and Astronautics* 17*th Aerospace Sciences Meeting*, *New Orleans*, *LA*, 15–17. *January*. Modal propagation angles in a cylindrical duct with flow and their relation to sound radiation.
10. S. T. Hocter 1999 *Journal of Sound and Vibration* **227**, 397–407. Exact and approximate directivity patterns of the sound radiated from a cylindrical duct.
11. J. B. Keller 1957 *Journal of Applied Physics* **28**, 426–444. Diffraction by an aperture I.
12. J. B. Keller 1962 *Journal of Optical Society of America* **52**, 116–130. Geometrical theory of diffraction.
13. R. G. Kouyoumjian and P. H. Pathak 1974 *Proceedings of the IEEE* **62**, 1448–1461. A uniform geometrical theory of diffraction for an edge in a perfectly conducting surface.
14. D. S. Ahluwalia, R. M. Lewis and J. Boersma 1968 *SIAM Journal of Applied Maths* **16**, 783–807. Uniform asymptotic theory of diffraction by a plane screen.
15. N. C. Albertsen, P. Balling and N. E. Jensen 1977 *IEEE Transactions on Antennas and Propagation* **AP-25**, 297–303. Caustics and caustic corrections to the field diffracted by a curved edge.
16. H. Y. Yee and L. B. Felsen 1969 *IEEE Transactions on Microwave Theory and Techniques* **MTT-17**, 73–85. Ray optics—a novel approach to scattering of discontinuities in a waveguide.
17. S. T. Hocter 1999 *Ph.D. Thesis*, *University of Keele*. Sound radiation from a cylindrical duct.
18. J. J. Bowman, T. B. A. Senior and P. L. E. Uslenghi 1987 *Electromagnetic and Acoustic Scattering from Simple Shapes*. New York: Harper and Row.